InxGa1-xP Nanowire Growth Dynamics Strongly Affected by Doping Using Diethylzinc

Otnes, Gaute; Heurlin, Magnus; Zeng, Xulu; Borgström, Magnus T.

Published in:
Nano Letters

DOI:
10.1021/acs.nanolett.6b03795

2017

Document Version:
Peer reviewed version (aka post-print)

$In_xGa_{1-x}P$ Nanowire Growth Dynamics Strongly Affected by Doping Using Diethylzinc

Gaute Otnes[*], *Magnus Heurlin*[†], *Xulu Zeng, and Magnus T. Borgström.*

Division of Solid State Physics and NanoLund, Lund University, P.O. Box 118, SE-221 00 Lund, Sweden

[†]Current affiliation: SolVoltaics AB, Scheelevägen 22, SE-22363 Lund, Sweden

TABLE OF CONTENTS GRAPHICS

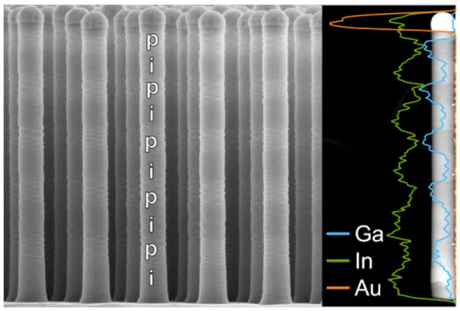

ABSTRACT Semiconductor nanowires are versatile building blocks for optoelectronic devices, in part because nanowires offer an increased freedom in material design due to relaxed constraints on lattice matching during the epitaxial growth. This enables the growth of ternary alloy nanowires in which the bandgap is tunable over a large energy range, desirable for optoelectronic devices. However, little is known about the effects of doping in the ternary nanowire materials, a pre-requisite for applications. Here we present a study of p-doping of $In_xGa_{1-x}P$ nanowires and show that the growth dynamics are strongly affected when diethylzinc is used as a dopant precursor.

Specifically, using in-situ optical reflectometry and high-resolution transmission electron microscopy we show that the doping results in a smaller nanowire diameter, a more predominant zincblende crystal structure, a more Ga-rich composition and an increased axial growth rate. We attribute these effects to changes in seed particle wetting angle and increased TMGa pyrolysis efficiency upon introducing diethylzinc. Lastly, we demonstrate degenerate p-doping levels in $In_xGa_{1-x}P$ nanowires by the realization of an Esaki tunnel diode. Our findings provide insights into the growth dynamics of ternary alloy nanowires during doping, thus potentially enabling the realization of such nanowires with high compositional homogeneity and controlled doping for high-performance optoelectronics devices.

KEYWORDS: Nanowire, doping, MOVPE, ternary compound, InGaP, crystal structure

There has recently been an increasing interest in using semiconductor nanowires to create optoelectronic devices, such as light emitting diodes,[1] lasers,[2] photodetectors[3] and solar cells,[4, 5] with potentially enhanced performance and lower cost. Due to relaxed lattice matching requirements, nanowires offer an increased freedom in materials design such that nanowire heterostructures of materials which are incompatible in planar technology can be synthesized,[6] and nanowires can be integrated monolithically on foreign substrates such as Si[7] and graphene.[8, 9] Further, by tuning the composition of ternary III-V compound nanowires, materials with bandgaps that corresponds to the main part of the solar spectrum can be accessed and combined. This enables the realization of nanowire-based multi-junction solar cells[10] where each junction absorbs a different part of the solar spectrum. For the successful development of such devices, a key requirement is the ability to control material conductivity through impurity doping. However, while

a lot of effort has been put into understanding doping of binary compound nanowires,[11] there is a need for better understanding and control of the doping of ternary nanowires, where the additional precursor is expected to introduce increased complexity in the growth dynamics.

In this Letter we present a study on the doping of $In_xGa_{1-x}P$ by diethylzinc (DEZn). For InP nanowires it has been shown that DEZn can strongly affect the nanowire growth dynamics, both with respect to crystal structure, diameter and growth rates.[12-14] We show how similar effects are present in the growth of $In_xGa_{1-x}P$, where introducing DEZn leads to a smaller nanowire diameter and a predominant zincblende (ZB) crystal structure. In addition we see a strong effect on the nanowire composition, the nanowires being significantly more Ga-rich when synthesized in the presence of DEZn. We show that this is driven by a more efficient incorporation of Ga, which we attribute to more efficient TMGa pyrolysis in the presence of DEZn. Finally, by the realization of an Esaki-tunnel diode we show that we are able to grow degenerately doped p-type $In_xGa_{1-x}P$, crucial for the successful realization of nanowire based optoelectronic devices. The $In_xGa_{1-x}P$ nanowires under study are grown in a composition range giving a direct bandgap suitable for use in nanowire based multi-junction solar cells and red LEDs.

Nanowires were grown from arrays of Au seed particles defined by nanoimprint lithography on full 2" InP:Zn (111)B wafers.[15] The seed particles were placed in the form of gold discs (diameter 190 nm and height 65 nm) in a hexagonal pattern optimized for light absorption,[16] with a center-to-center distance of 500 nm. The hexagonal pattern ensures that all nanowires have an equal collection area for diffusing growth precursors. For ternary compounds, such as $In_xGa_{1-x}P$, this is expected to be especially important in order to achieve homogeneous and reliable growth, since big differences might exist in migration length of the group III growth species.[17] Imprinted growth substrates cleaved into approximately 0.6 x 0.6 cm^2 sizes were placed in a laminar flow MOVPE

reactor (Aixtron 200/4), which used H_2 as a carrier gas, a total gas flow of 13 l/min and a working pressure of 100 mbar. Prior to growth, the substrates were subjected to an in situ pre-anneal nucleation scheme[15] at 280 °C. This reduces Au seed particle displacement during the following 10 minute annealing at 550 °C performed in a PH_3/H_2-ambient to desorb surface oxides. The growth chamber was then cooled to the growth temperature of 440 °C. The nanowires were nucleated with an InP segment grown for one minute, using phosphine and trimethylindium (TMIn) at precursor molar fractions of $\chi_{PH3} = 6.9\times10^{-3}$ and $\chi_{TMIn} = 8.9\times10^{-5}$. After 15 seconds HCl was added to the gas mixture at a molar fraction of $\chi_{HCl} = 4.6\times10^{-5}$ to suppress radial growth.[18, 19] After one minute of InP growth, growth of $In_xGa_{1-x}P$ was initiated by adding trimethylgallium (TMGa) at a molar fraction of $\chi_{TMGa} = 4.0\times10^{-4}$, changing the TMIn flow to $\chi_{TMIn} = 5.2\times10^{-5}$, and increasing HCl to $\chi_{HCl} = 5.4\times10^{-5}$. Growth was terminated by switching off all precursor gas flows except PH_3 and cooling the reactor in a PH_3/H_2 gas mixture. This procedure to grow $In_xGa_{1-x}P$ nanowires was the same for all samples under study here.

To properly assess the complex influence of adding DEZn to the precursor flow, two different doping schemes were applied together with the standard growth procedure. First, a barcode structure with a sequential variation between nominally intrinsic ($\chi_{DEZn} = 0$) and highly p-doped ($\chi_{DEZn} = 4.3\times10^{-5}$) material was grown. The first segment was nominally intrinsic and a total of 5 alternating i-p segments were grown sequentially. The growth time for each nominally intrinsic and p-doped segment was 140 s and 110 s, respectively. Second, six samples of homogeneously doped nanowires were grown with a constant DEZn molar fraction through the nanowire. This was varied in the range $\chi_{DEZn} = 0$ to 4.3×10^{-5} between the different samples.

The heterostructured p-$In_xGa_{1-x}P$/n-InP nanowires containing an Esaki tunnel diodes were grown at 440 °C to a total length of ~2 µm. On top of an initial InP segment, grown for one minute as

described previously, the 1 µm long p-$In_xGa_{1-x}P$ segment was grown using the same molar fractions as in the standard growth procedure described above, with $\chi_{DEZn} = 8.3\times10^{-5}$. Thereafter, the 1 µm long n-InP segment was grown using molar fractions of $\chi_{PH3} = 6.9\times10^{-3}$, $\chi_{TMIn} = 5.9\times10^{-5}$, $\chi_{H2S} = 0.2\times10^{-5}$ and $\chi_{HCl} = 4.6\times10^{-5}$. For the ~30 nm of the p- and n-segments closest to the heterojunction, dopant molar fractions were increased to $\chi_{DEZn} = 11.7\times10^{-5}$ and $\chi_{H2S} = 1.6\times10^{-5}$, respectively.

During growth, a LayTec EpiR DA UV optical reflectometry system attached to the Aixtron reactor was used to monitor the nanowire length and growth rate in-situ.[14] We used wavelengths in the range between 500 and 700 nm to calculate the nanowire length, giving us on average 2-3 datapoints per second. As in ref.14, an effective refractive index (see Supporting Information) was used for the length calculations, determined empirically as an average from calibration runs where InP nanowires were grown using the same pattern of catalyst particles. The use of this effective refractive index also for $In_xGa_{1-x}P$ nanowires was validated on the homogeneously doped $In_xGa_{1-x}P$ nanowires by comparing optical reflectometry length data with average lengths measured by scanning electron microscopy (SEM) after growth. For all samples the lengths obtained by the two methods was within 5% (most within 3%), similar to what is seen for growth of pure InP nanowires. Further, no trends were seen in the data as a function of nanowire composition when it comes to accuracy of the used refractive index, indicating that the effective refractive index of the nanowire array does not change substantially within the composition range studied here. This is to be expected, since the difference in refractive index between InP and GaP in our wavelength range is small.[20] Additionally, the effect of the nanowire refractive index is limited, since the reflected light travels through an array consisting mostly of ambient gas, as confirmed by the determined effective refractive index being close to 1 (see Supporting Information).

After growth, the nanowires were examined using SEM and transmission electron microscopy (TEM). For high resolution TEM (HRTEM) investigations, nanowires were transferred to a holey carbon TEM grid by sliding the grid gently over a portion of the center of the grown sample. Energy dispersive x-ray spectroscopy (XEDS) was used in the TEM to gather information about the nanowire composition. Before transferring some of the nanowires to the TEM grid, the composition of a larger nanowire ensemble on each sample was assessed by x-ray diffraction (XRD). The nanowire composition was extracted from the XRD peaks by assuming Vegard's law, and the full-width-at-half-maximum (FWHM) was taken as a measure of the compositional variation.

For electrical measurements, nanowires were broken off from the growth substrate and deposited on a degenerately doped Si substrate which had a thermally grown SiO_2 layer on top. After the deposition, metal contacts were defined to single nanowires by electron beam lithography, metal evaporation and lift-off. The metal contact layers used were Ti/Zn/Au (5/20/150 nm nominal thickness) to p-$In_xGa_{1-x}P$ segments and Ti/Au (5/20 nm nominal thickness) for n-InP segments. All electrical measurements were performed in a probe station.

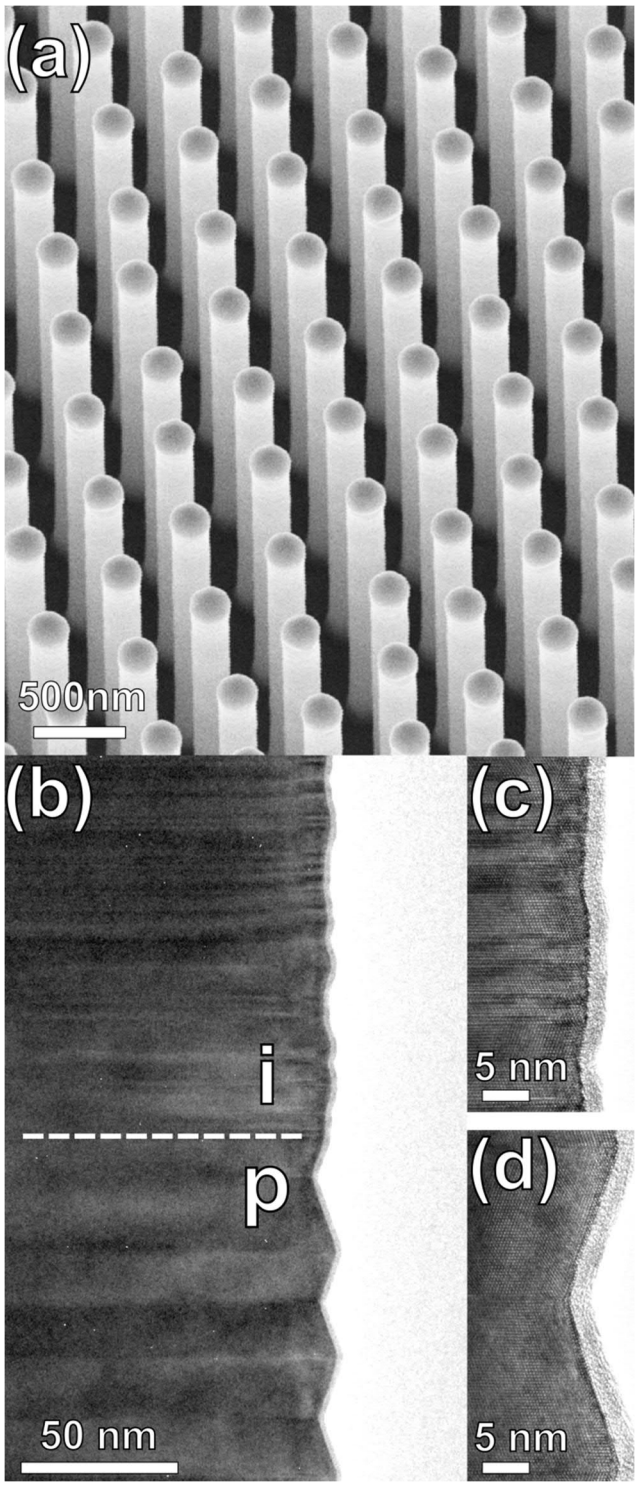

Figure 1 Adding DEZn to the precursor flow induces a change in crystal structure towards more zincblende. (a) Scanning electron microscope image of as-grown $In_xGa_{1-x}P$ nanowires with a barcoded DEZn doping scheme. (b) High-resolution transmission electron

microscopy image (obtained along the [1-10] zone axis) taken at the interface between two segments in the barcoded structure, grown without (top part, high magnification in (c)) and with (bottom part, high magnification in (d)) DEZn.

We take a first step to understand the growth dynamics of our Zn-doped $In_xGa_{1-x}P$ nanowires by studying their morphology and crystal structure. SEM images of the nanowires grown with a barcode doping scheme shows that the nanowires have a diameter just below 200 nm and a length of about 2 µm (Figure 1a). For all samples grown we achieved a high yield of more than 99 % vertical $In_xGa_{1-x}P$ nanowires in our dense pattern (see Supporting Information), critical for implementation into nanowire array optoelectronic devices. The crystal structure of the nanowires was investigated by HRTEM (Figure 1b-d), and we observed that adding DEZn to the precursor flow induces a change in crystal structure towards more zincblende (ZB), similar to results on p-doping of binary InP and GaP nanowires using DEZn by Algra et al.[12, 21] In the homogeneously doped nanowires we also observe a diameter decrease from 198 ± 2 nm for the nominally intrinsic nanowires to 187 ± 2 nm for the highest doped (χ_{DEZn}= 4.3×10^{-5}), as measured by SEM (see Supporting Information). These two effects are related since the wetting angle of the Au particle (which affects the diameter) is directly linked to the crystal structure.[12, 13, 22, 23] We note that the barcoded nanowires show a somewhat less pronounced diameter change than the homogeneously doped nanowires, with diameters measured to 196 ± 2 nm and 191 ± 2 nm for the nominally intrinsic and the p-doped segments, respectively. We now turn our attention to the effect of DEZn on group III incorporation.

VLS-growth of ternary III-V nanowires is a complex process[17, 19, 24-27] and for $In_xGa_{1-x}P$ nanowires the relative efficiency of Ga and In incorporation is governed by several factors which are interdependent. Both the relative decomposition efficiency of group III precursor molecules and relative group III adatom migration lengths on the substrate surface and nanowire sidewalls are expected to affect the composition of the solid,[27] and may result in inhomogeneous materials composition along the nanowire. Additional complexity is added by gas phase diffusion of partially decomposed precursor molecules between nearby nanowires.[28] The commonly seen variation in ternary nanowire composition from competition between axial VLS growth and radial vapor-solid growth [24-26] is less relevant here since HCl effectively suppresses radial growth (Figure 1a).

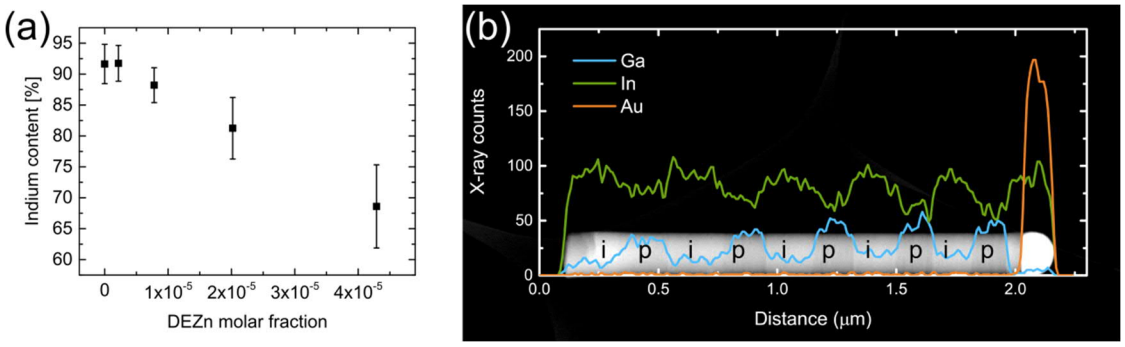

Figure 2 Composition changes to more Ga-rich $In_xGa_{1-x}P$ nanowires when adding DEZn. (a) Composition extracted from x-ray diffraction (XRD) from an ensemble of homogeneously doped $In_xGa_{1-x}P$ nanowires, at different DEZn molar fractions. Error bars indicate full-width-at-half-maximum of the XRD-peak. For XRD raw data, see Supporting Information. (b) Energy dispersive x-ray spectroscopy scan of a barcoded $In_xGa_{1-x}P$ nanowire. The nanowire composition changes in a reversible fashion to more Ga-rich when growing in the presence of DEZn.

The addition of DEZn to the growth chamber leads to more Ga-rich nanowires (Figure 2). At our growth temperature (440 °C), the longer surface migration length of In-species[17] combined with the lower decomposition temperature of TMIn[29] as compared to TMGa,[30] result in more efficient In than Ga incorporation. This is reflected in our XRD data of the homogeneously doped nanowires (Figure 2a), where a gas phase precursor ratio of $\chi_{TMIn}/(\chi_{TMGa}+\chi_{TMIn}) = 0.12$ gives almost pure InP nanowires ($x = 0.92 \pm 0.03$) for the nominally intrinsic $In_xGa_{1-x}P$ nanowires. The Ga to In incorporation changes as more DEZn is added to the precursor gas flow, observable in our experiments for $\chi_{DEZn} \geq 0.8\times10^{-5}$ (Figure 2a), reaching $x = 0.69 \pm 0.07$ when $\chi_{DEZn} = 4.3\times10^{-5}$. As revealed by XEDS scans of a barcoded nanowire (Figure 2b), this effect is reversible; the composition switches back and forth following the on/off switching of the DEZn flow.

To better understand the effects of DEZn on nanowire composition we employed in-situ monitoring with optical reflectometry[14] while growing our structures. Figure 3a shows the barcoded nanowire length as a function of growth time (see Supporting information for a zoom-in of two neighboring segments, including linear fits). The growth rates are plotted in Figure 3b, as extracted for each segment by linear fits to the data in Figure 3a. A small but clear increase in axial growth rate of about 10-15 % is observed when adding DEZn, accompanying the compositional change (Figure 2b). In Figure 3c, volume growth rates for the “InP” and “GaP” components of each segment is shown (see Supporting Information for details on calculation). Two observations can be made by comparing Figure 3b and 3c. First, we observe an overall decreasing trend in axial growth rate for both the p- and the i-segments (Figure 3b), which stems from a steadily decreasing incorporation of In as the nanowire length increases (Figure 3c). Thus, the incorporation of In is limited by surface migration of In species on the substrate and nanowire sidewalls. Second, the

higher axial growth rate in the p-segments (Figure 3b) originates from an increased incorporation of Ga (Figure 3c).

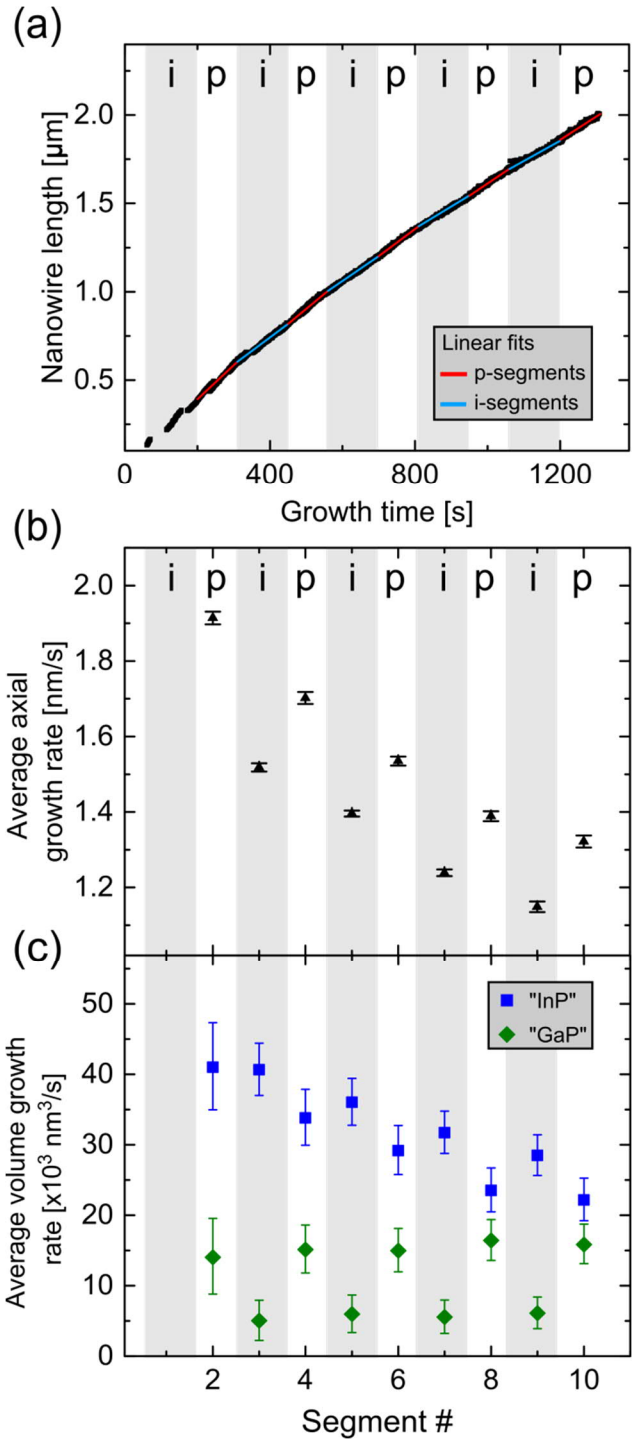

Figure 3 Axial $In_xGa_{1-x}P$ nanowire growth rate increases when adding DEZn, due to an increased Ga-incorporation. (a) $In_xGa_{1-x}P$ nanowire length vs growth time extracted from in-situ optical reflectometry data, for a barcoded doping scheme. Lengths extracted during growth of nominally intrinsic material and p-doped material are indicated by shaded and non-shaded areas, respectively. Linear fits to the length vs growth time data in each segment is shown by blue and red lines, for the nominally intrinsic and the p-doped segments respectively. (b) Average growth rate for each nominally intrinsic (shaded area) and p-doped (non-shaded area) segment, extracted by the linear fits to length vs growth time data in (a). Error bars indicate one standard error in the fit. (c) Volume growth rates for the "InP" (blue squares) and "GaP" (green diamonds) components of each nominally intrinsic (shaded area) and p-doped (non-shaded area) segment. The volume growth rate was calculated from three input parameters: composition, axial growth rate, and diameter. The error bars indicate the maximum and minimum values possible within the errors of the input parameters (see Supporting Information for details on determination of input parameters).

In the following we consider several possible explanations to the increased Ga incorporation. First, DEZn changes the interface energies in the system (as evidenced by the change in diameter and crystal structure) which could be thought to block or enhance the uptake of In or Ga, respectively. However, we observed that the growth rate was strongly dependent on the precursor flows, which indicate that Ga and/or In uptake in the particle or at the growth front is not limiting the growth. Another possibility is that the change in crystal structure induced by DEZn (Figure 1b) could result in changed surface migration lengths which affect both growth rates and composition. This option must however be discarded due to the reversibility of the process as shown by the barcoded structure (Figure 2b). A more likely explanation is then a change in surface migration

lengths due to surface passivation effects, which has been used to explain nanowire growth rate changes both for Zn[14] and other dopants.[31, 32] However, the constant trend in Ga incorporation rate for both the p- and i-segments with increasing nanowire length (Figure 3c) indicates that the Ga incorporation is not limited by adatom migration. Further, a passivated surface should affect migration of both In- and Ga-species, and cannot be used to explain the higher growth rate which we observe is predominantly driven by increased Ga incorporation. Instead we attribute the composition and growth rate changes to an enhanced pyrolysis efficiency of TMGa when adding DEZn. While TMIn is fully pyrolyzed at our growth temperature of 440 °C,[29, 33] this is not the case for TMGa.[30] Methyl radicals have been proposed to react with the H_2 ambient and create H-radicals attacking the TMGa molecule, thereby increasing its pyrolysis rate.[30, 34] We speculate that the extra ethyl radicals added from pyrolyzed DEZn[35, 36] could have a similar effect, since the ethyl and methyl radical reactions with H_2 have comparable activation energies (values ranging from ~ 40 to 60 kJ/mol have been reported for both[34, 37]). The methyl groups released from additional pyrolyzed TMGa could further enhance the process through a chain reaction.[30] An increased efficiency of TMGa pyrolysis would lead to a higher supply of Ga atoms at the growth front, and in a reversible fashion result in more Ga-rich material and an increased growth rate.

It should be noted that effects of DEZn on group III incorporation have been seen in several studies of ternary and quaternary compound layer growth, as summarized by Li et.al.[38] These results were obtained at significantly higher growth temperatures (≥ 550 °C) where the group III precursors are fully pyrolyzed and were explained with a decreased efficiency of In incorporation due to increased In desorption at high temperature and competition between In and Zn incorporation to the group III position in the lattice.[38] Zn competes more easily with In atoms than Ga atoms because the binding energy of Ga-P is much higher than that of In-P. In contrast to the

results on layer growth, for kinetically limited nanowire growth we find that DEZn increases the incorporation efficiency of Ga, which we explain by enhanced pyrolysis of TMGa related species.

We note that the XRD peaks (Figure 2a and Supporting Information) indicate a certain compositional variation in the measured nanowires, which increases as more DEZn is added to the growth chamber (the nanowires become more Ga-rich). By studying the XEDS scan shown in Figure 2b, we see that the nanowire composition gets significantly more Ga-rich towards the top of the nanowire. Comparing this with Figure 3c, we conclude that the Ga content increases towards the top of the nanowires due to a decreased incorporation of In, limited by surface migration, and that the width of the XRD peaks is mainly due to a variation in composition along the length of the nanowire. Further, in both the p- and the nominally intrinsic segments, we observe almost a doubling of the Ga-content from the bottom to the top segment (Figure 2b). Since the Ga-content near the bottom of the nanowire is much higher in the p-segment than in the nominally intrinsic segment, the increase in Ga-content along the nanowire is significantly larger in absolute numbers for the p-doped segments. This translates to a broader XRD-peak and larger compositional inhomogeneity in the homogeneously doped nanowires with increasing DEZn (Figure 2a). Such compositional variation along the length of the nanowires can be suppressed by in-situ tuning of the group III precursor flow during growth.[39]

Our results demonstrate the complex nature of ternary III-V nanowire growth and doping. To further progress towards real devices, control and knowledge of actual doping levels are needed. In order to evaluate zinc doping levels in our $In_xGa_{1-x}P$ nanowires, single homogeneously doped nanowires were contacted for electrical measurements. Due to challenges in forming Ohmic contacts to p-type $In_xGa_{1-x}P$ nanowires, similar to what has been seen for p-type InP nanowires,[31,

[40] the I-V curve obtained from such devices was dominated by the poor contacts for all measured nanowires, regardless of DEZn molar fraction. Poor gate response was observed in gate dependent measurement, preventing accurate assessment of the carrier concentration, even though p-type behavior was seen. Taking another trail, nanowires with a p-$In_xGa_{1-x}P$ / n-InP axial heterojunction were grown and contacted with the aim to form an Esaki tunnel diode (Figure 4). The materials composition of the p-$In_xGa_{1-x}P$ segment in this heterojunction was determined by XRD after growth to be $x = 0.69 \pm 0.03$.

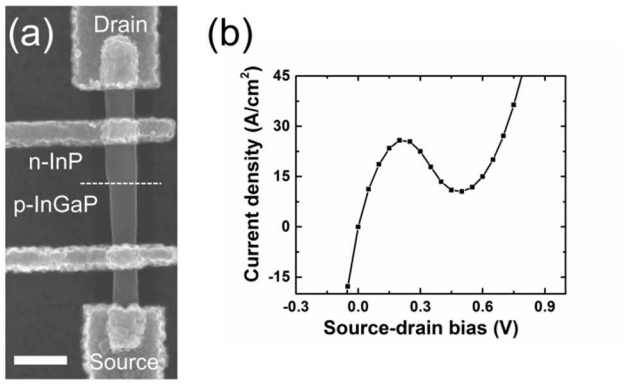

Figure 4 Realization of a nanowire Esaki diode demonstrate degenerate p-doping in $In_xGa_{1-x}P$ nanowires. (a) Top-view SEM image of a contacted p-$In_xGa_{1-x}P$ / n-InP Esaki diode nanowire. As indicated in the figure, the bottom segment (~ 1 µm) is $In_xGa_{1-x}P$ doped with DEZn, while the top segment (~ 1 µm) is InP degenerately doped by use of H_2S. The Esaki diode is formed at the $In_xGa_{1-x}P$ / InP heterojunction, indicated by the dotted line. The extra perpendicular contacts were added to give the ability to electrically characterize each segment separately. Scale bar is 500 nm. (b) I-V sweep of a p-$In_xGa_{1-x}P$ / n-InP nanowire Esaki diode.

Despite poor contact characteristics at the p-type $In_xGa_{1-x}P$ side, the I-V curve of a typical p-$In_xGa_{1-x}P$ /n-InP nanowire still shows clear negative differential resistance (NDR) region, revealing the existence of a tunneling effect (Figure 4b shows the best device measured). Based on our

previous doping evaluation study,[41] the n-type InP side was degenerately doped. p-doping by use of DEZn up to degenerate level was thus demonstrated in our $In_xGa_{1-x}P$ nanowires. Detailed investigations of $In_xGa_{1-x}P$ / InP nanowire Esaki diodes will be reported elsewhere.

In summary, we have systematically studied the effect of p-doping $In_xGa_{1-x}P$ nanowire by use of DEZn as a dopant precursor. By combining HRTEM, SEM and in-situ optical reflectometry we observe that the presence of DEZn during synthesis changes the growth dynamics of the $In_xGa_{1-x}P$ nanowires and induces a smaller nanowire diameter and ZB crystal structure, an increased axial growth rate and a more Ga-rich composition. We attribute the changes in nanowire diameter and crystal structure to changes in the wetting angle of the Au seed particle, similar to what has been observed for InP nanowires. The increased axial growth rate and the more Ga-rich composition can be explained by an enhanced pyrolysis of TMGa in the presence of ethyl radicals from decomposed DEZn. Finally, by realizing $In_xGa_{1-x}P$ /InP nanowire Esaki diodes we demonstrate that high p-doping is possible in $In_xGa_{1-x}P$ nanowires by use of DEZn. These results provide a stepping stone towards harvesting the full potential of ternary compound nanowires in optoelectronic devices.

ASSOCIATED CONTENT

Supporting Information

Details on methodology and calculations, and XRD raw data.

AUTHOR INFORMATION

Corresponding Author

*E-mail: gaute.otnes@ftf.lth.se

Author Contributions

The manuscript was written through contributions from all authors. All authors have given approval to the final version of the manuscript.

Notes

The authors declare no competing financial interests.

ACKNOWLEDGEMENTS

This work was performed within NanoLund and supported by the Swedish Research Council (Vetenskapsrådet), the Swedish Foundation for Strategic Research (SSF), the Knut and Alice Wallenberg Foundation and the Swedish Energy Agency. This project has received funding from the *European Union's Horizon 2020 research and innovation programme* under grant agreement No 641023 (Nano-Tandem) and the *European Union's FP7 programme* under grant agreement No 608153 (PhD4Energy). This publication reflects only the author's views and the funding agency is not responsible for any use that may be made of the information it contains.

The authors thank Dr. Filip Lenrick and Professor Reine Wallenberg for help with TEM measurements, and Dr. Masoomeh Ghasemi for helpful discussions.

REFERENCES

1. Gudiksen, M. S.; Lauhon, L. J.; Wang, J.; Smith, D. C.; Lieber, C. M. Nature 2002, 415, (6872), 617-620.
2. Huang, M. H.; Mao, S.; Feick, H.; Yan, H. Q.; Wu, Y. Y.; Kind, H.; Weber, E.; Russo, R.; Yang, P. D. Science 2001, 292, (5523), 1897-1899.
3. Wei, W.; Bao, X. Y.; Soci, C.; Ding, Y.; Wang, Z. L.; Wang, D. Nano Lett 2009, 9, (8), 2926-2934.
4. Wallentin, J.; Anttu, N.; Asoli, D.; Huffman, M.; Åberg, I.; Magnusson, M. H.; Siefer, G.; Fuss-Kailuweit, P.; Dimroth, F.; Witzigmann, B.; Xu, H. Q.; Samuelson, L.; Deppert, K.; Borgström, M. T. Science 2013, 339, (6123), 1057-1060.
5. Åberg, I.; Vescovi, G.; Asoli, D.; Naseem, U.; Gilboy, J. P.; Sundvall, C.; Dahlgren, A.; Svensson, K. E.; Anttu, N.; Björk, M. T.; Samuelson, L. Ieee J Photovolt 2015, 6, (1), 185-190.
6. Björk, M.; Ohlsson, B.; Sass, T.; Persson, A.; Thelander, C.; Magnusson, M.; Deppert, K.; Wallenberg, L.; Samuelson, L. Appl Phys Lett 2002, 80, (6), 1058-1060.

7. Mårtensson, T.; Svensson, C. P. T.; Wacaser, B. A.; Larsson, M. W.; Seifert, W.; Deppert, K.; Gustafsson, A.; Wallenberg, L. R.; Samuelson, L. Nano Lett 2004, 4, (10), 1987-1990.
8. Hong, Y. J.; Lee, W. H.; Wu, Y. P.; Ruoff, R. S.; Fukui, T. Nano Lett 2012, 12, (3), 1431-1436.
9. Munshi, A. M.; Dheeraj, D. L.; Fauske, V. T.; Kim, D. C.; van Helvoort, A. T. J.; Fimland, B. O.; Weman, H. Nano Lett 2012, 12, (9), 4570-4576.
10. LaPierre, R. R.; Chia, A. C. E.; Gibson, S. J.; Haapamaki, C. M.; Boulanger, J.; Yee, R.; Kuyanov, P.; Zhang, J.; Tajik, N.; Jewell, N.; Rahman, K. M. A. Phys Status Solidi-R 2013, 7, (10), 815-830.
11. Wallentin, J.; Borgström, M. T. J Mater Res 2011, 26, (17), 2142-2156.
12. Algra, R. E.; Verheijen, M. A.; Borgström, M. T.; Feiner, L. F.; Immink, G.; van Enckevort, W. J. P.; Vlieg, E.; Bakkers, E. P. A. M. Nature 2008, 456, (7220), 369-372.
13. Wallentin, J.; Ek, M.; Wallenberg, L. R.; Samuelson, L.; Deppert, K.; Borgström, M. T. Nano Lett 2010, 10, (12), 4807-4812.
14. Heurlin, M.; Anttu, N.; Camus, C.; Samuelson, L.; Borgström, M. T. Nano Lett 2015, 15, (5), 3597-3602.
15. Otnes, G.; Heurlin, M.; Graczyk, M.; Wallentin, J.; Jacobsson, D.; Berg, A.; Maximov, I.; Borgström, M. T. Nano Res 2016, doi:10.1007/s12274-016-1165-z.
16. Anttu, N.; Xu, H. Q. Opt Express 2013, 21, (9), A558-A575.
17. Kim, Y.; Joyce, H. J.; Gao, O.; Tan, H. H.; Jagadish, C.; Paladugu, M.; Zou, J.; Suvorova, A. A. Nano Lett 2006, 6, (4), 599-604.
18. Borgström, M. T.; Wallentin, J.; Trägårdh, J.; Ramvall, P.; Ek, M.; Wallenberg, L. R.; Samuelson, L.; Deppert, K. Nano Res 2010, 3, (4), 264-270.
19. Jacobsson, D.; Persson, J. M.; Kriegner, D.; Etzelstorfer, T.; Wallentin, J.; Wagner, J. B.; Stangl, J.; Samuelson, L.; Deppert, K.; Borgström, M. T. Nanotechnology 2012, 23, (24), 245601.
20. Adachi, S. J Appl Phys 1989, 66, (12), 6030-6040.
21. Algra, R. E.; Verheijen, M. A.; Feiner, L.-F.; Immink, G. G. W.; Enckevort, W. J. P. v.; Vlieg, E.; Bakkers, E. P. A. M. Nano Lett 2011, 11, (3), 1259-1264.
22. Glas, F.; Harmand, J.-C.; Patriarche, G. Phys Rev Lett 2007, 99, (14), 146101.
23. Jacobsson, D.; Panciera, F.; Tersoff, J.; Reuter, M. C.; Lehmann, S.; Hofmann, S.; Dick, K. A.; Ross, F. M. Nature 2016, 531, (7594), 317-322.
24. Chen; Shehata, S.; Fradin, C.; LaPierre, R.; Couteau, C.; Weihs, G. Nano Lett 2007, 7, (9), 2584-2589.
25. Lim, S. K.; Tambe, M. J.; Brewster, M. M.; Gradecak, S. Nano Lett 2008, 8, (5), 1386-1392.
26. Fakhr, A.; Haddara, Y.; LaPierre, R. Nanotechnology 2010, 21, (16), 165601.
27. Ameruddin, A.; Caroff, P.; Tan, H. H.; Jagadish, C.; Dubrovskii, V. Nanoscale 2015, 7, (39), 16266-16272.
28. Borgström, M. T.; Immink, G.; Ketelaars, B.; Algra, R.; Bakkers, E. P. A. M. Nat Nanotechnol 2007, 2, (9), 541-544.
29. Buchan, N. I.; Larsen, C. A.; Stringfellow, G. B. J Cryst Growth 1988, 92, (3-4), 591-604.
30. Larsen, C. A.; Buchan, N. I.; Li, S. H.; Stringfellow, G. B. J Cryst Growth 1990, 102, (1-2), 103-116.
31. Borgström, M. T.; Wallentin, J.; Heurlin, M.; Fält, S.; Wickert, P.; Leene, J.; Magnusson, M. H.; Deppert, K.; Samuelson, L. Ieee J Sel Top Quant 2011, 17, (4), 1050-1061.
32. Wallentin, J.; Mergenthaler, K.; Ek, M.; Wallenberg, L. R.; Samuelson, L.; Deppert, K.; Pistol, M. E.; Borgström, M. T. Nano Lett 2011, 11, (6), 2286-2290.
33. Buchan, N. I.; Larsen, C. A.; Stringfellow, G. B. J Cryst Growth 1988, 92, (3), 605-615.
34. Lee, P. W.; Omstead, T. R.; McKenna, D. R.; Jensen, K. F. J Cryst Growth 1987, 85, (1), 165-174.
35. Koski, A. A.; Price, S. J. W.; Trudell, B. C. Can J Chem 1976, 54, (3), 482-487.
36. Kim, Y. S.; Won, Y. S.; Hagelin-Weaver, H.; Omenetto, N.; Anderson, T. The Journal of Physical Chemistry A 2008, 112, (18), 4246-4253.

37. Kondratiev, V. N., Rate constants of gas phase reactions; reference book. Office of Standard Reference Data, National Bureau of Standards, U.S. Dept. of Commerce; distributed by National Technical Information Service, Springfield, Va.: Washington,, 1972; p vi, 428 p.
38. Li, X. Y.; Zhang, J. Q.; Zhang, W.; Lu, H. B.; Zhou, D. Y. Thin Solid Films 2015, 592, 24-28.
39. Berg, A.; Lenrick, F.; Vainorius, N.; Beech, J. P.; Wallenberg, L. R.; Borgström, M. T. Nanotechnology 2015, 26, (43), 4356011-4356018.
40. Wallentin, J.; Wickert, P.; Ek, M.; Gustafsson, A.; Reine Wallenberg, L.; Magnusson, M. H.; Samuelson, L.; Deppert, K.; Borgström, M. T. Appl Phys Lett 2011, 99, (25), 253105.
41. Hultin, O.; Otnes, G.; Borgström, M. T.; Björk, M.; Samuelson, L.; Storm, K. Nano Lett 2016, 16, (1), 205-211.